Available online at www.sciencedirect.com
SCIENCE DIRECT®
Journal of Solid State Chemistry 173 (2003) 299–308
JOURNAL OF SOLID STATE CHEMISTRY
http://elsevier.com/locate/jssc

The defect chemistry of $La_{1-\Delta}MnO_{3+\delta}$

Keikichi Nakamura*,[1]

Graduate School of Integrated Science, Yokohama City University, Yokohama 2360027, Japan

Received 7 October 2002; received in revised form 10 January 2003; accepted 18 January 2003

Abstract

The effects of oxygen reduction treatments on the magnetic properties of La-deficient manganites, $La_{1-\Delta}MnO_{3+\delta}$ and Sr- and Ca-doped manganites, $La_{1-x}M_xMnO_{3+\delta}$ (M: Sr, Ca) have been investigated to confirm the contrasting oxygen reduction effects on the magnetization properties. It is found that oxygen reduction treatments in reduced oxygen pressures of 10^3–1 Pa for $La_{1-\Delta}MnO_{3+\delta}$ result in a continuous change in the magnetization but the reduction treatments for $La_{1-x}M_xMnO_{3+\delta}$ result in a negligible change under the same reduction conditions. To interpret the contrasting behavior of the La-deficient manganites, several possible models have been discussed. Among the models, the most probable model is that vacancies generated by the La deficiency Δ are partially replaced by $\Delta_2(=\Delta-\Delta_1\leqslant\Delta_1)$ Mn ions to give both La and Mn site vacancies according to the formula $La_{1-\Delta}V_\Delta MnO_{3+\delta}\rightarrow\{La_{1-\Delta}Mn_{\Delta_2}V_{\Delta_1}\}\{Mn_{1-\Delta_2}V_{\Delta_2}\}O_{3+\delta}$. Details of thermodynamic basis of this model have been presented.

Keywords: Defect chemistry; $LaMnO_3$; $La_{0.7}Sr_{0.3}MnO_3$; Lanthanum manganite; cmr; gmr; Perovskite; Cation vacancy

1. Introduction

In the doped $La_{1-x}M_xMnO_{3+\delta}$ (M:Sr, $x\leqslant0.3$) compounds prepared under conventional conditions (e.g., annealed in air at 1373 K and furnace cooled to RT), Mn^{4+} proportion is reported to be almost independent of doping level [1]. This phenomenon has been also recognized by the observed and calculated pressure–δ–temperature relation (P–δ isotherms) of $La_{1-x}Sr_xMnO_{3+\delta}$ bulk [2,3] and thin films [4]. These compounds, however, when heat-treated in a reducing atmosphere (annealed in Ar or in N_2 or in a controlled lower oxygen partial pressure), Mn^{4+} proportion decreases with increasing oxygen reduction and approaches the value characteristic of La site doping level, i.e. $[Mn^{4+}]=0.3$ for $x=0.3$, 0.2 for $x=0.2$ and so on [1,2,4,5]. As for the La-deficient $La_{1-\Delta}MnO_{3+\delta}$ compounds ($\Delta\leqslant0.1$), the maximum Mn^{4+} proportion is almost independent of the La-deficient level and is close to that for the Sr- and Ca-doped manganites, i.e., 0.3–0.36 [6,7]. If one assumes that in the $La_{1-\Delta}MnO_{3+\delta}$ compounds, vacancies are located in the La sites such as expressed by a formula, $La_{1-\Delta}V_\Delta MnO_{3+\delta}$, one can also expect that Mn^{4+} proportion decreases with the reduction of oxygen in the same manner as observed in the Sr-doped cases, i.e., approaches the value characteristic of the vacancy doping level, 0.3 for $\Delta=0.1$, 0.15 for $\Delta=0.05$, etc. This estimation is, however, different from the observed behavior that in the $La_{1-\Delta}MnO_{3+\delta}$ compounds with $\Delta=0$, 0.05 and 0.1, Mn^{4+} proportion less than 0.05 can be easily obtained independent of the La-deficient level Δ when reduced under the similar reduction conditions as those for the Sr-doped cases cited above [6–8].

Another problem in the La site vacancy doped model is the inconsistency with the established cation vacancy model [3,5,9] that excess oxygen generates equal amounts of vacancies both in the La and Mn sites. From the point of view of the defect exclusion models [10,11], it is hard to imagine that in the $La_{1-\Delta}V_\Delta MnO_{3+\delta}$ formula composition, excess oxygen generates vacancies in the La sites in addition to the La site vacancies Δ, because the proportion of La site vacancies exceed the upper limit value 0.0566, when $\Delta>0.0566$ (this value can be obtained by putting $x=0$ and $\delta=0.18$ into Eq. (2)). Recently [12], we have presented a systematic research on the contrasting effects of oxygen reduction treatments on thin films of $La_{1-\Delta}MnO_{3+\delta}$ and proposed a defect model to account for the observed effects. In the

*Fax: +81-29-859-2701.
E-mail address: keinaka@d9.dion.ne.jp.
[1] Present address: National Institute for Material Science, Sengen 1-2-1, Tsukuba 305-0047, Japan.

0022-4596/03/$ - see front matter
doi:10.1016/S0022-4596(03)00091-4

Table 1
Details of oxygen-reduction treatment, lattice parameters, unit-cell volume and estimated Mn^{4+} proportion for the samples shown in Figs. 4–7

Composition	Oxygen-reduction treatment	Lattice parameters	Unit-cell volume	Estimated Mn^{4+} proportion
$LaMnO_{3+\delta}$	1223 K, 10^5 Pa O_2	$a = 5.474$, $\alpha = 60.59$	235.1	0.29
$LaMnO_{3+\delta}$	1173 K, dynamic vac.	$a = 5.527$, $b = 5.694$, $c = 7.701$	242.36	0.06
$La_{0.92}MnO_{3+\delta}$	1273 K, 10^5 Pa O_2	$a = 5.477$, $\alpha = 60.54$	235.17	0.29
$La_{0.92}MnO_{3+\delta}$	1273 K, 1 Pa O_2	$a = 5.528$, $b = 5.678$, $c = 7.717$	242.23	0.067
$La_{0.96}MnO_{3+\delta}$	1273–1073 K, 10^5 Pa O_2	$a = 5.471$, $\alpha = 60.61$	234.75	0.31
$La_{0.96}MnO_{3+\delta}$	1273 K, 1170 Pa O_2	$a = 5.521$, $b = 5.538$, $c = 7.784$	237.98	Two phases[a]
$La_{0.96}MnO_{3+\delta}$	1273 K, 135 Pa O_2	$a = 5.520$, $b = 5.616$, $c = 7.728$	239.6	0.12
$La_{0.96}MnO_{3+\delta}$	1273 K, 1 Pa O_2	$a = 5.529$, $b = 5.689$, $c = 7.706$	242.4	0.06
$La_{0.96}MnO_{3+\delta}$	1273 K, dynamic vac.	$a = 5.526$, $b = 5.685$, $c = 7.701$	241.95	0.08

[a] Orthorhombic and rhombohedral phases coexist [8,11].

first part of this paper, similar contrasting effects of oxygen-reduction treatments on the magnetic properties of polycrystalline samples will be presented. In the second part, several possible defect models will be discussed to determine a thermodynamically reasonable and acceptable model to interpret consistency on the contrasting effects cited above. A detailed discussion on the La site Mn substitution for the most reasonable model will also be presented.

2. Experimental procedure

Polycrystalline bulk samples of $La_{1-\Delta}MnO_{3+\delta}$ ($\Delta = 0$, 0.04 and 0.08) and $La_{0.7}M_{0.3}MnO_{3+\delta}$ (M: Ca, Sr) were synthesized by the conventional solid-state reaction method [11]. The excess oxygen contents in the bulk polycrystalline samples were controlled by the same method described in detail in the previous papers [4,11]. The schematic diagram of the apparatus shown in Fig. 2 of the previous paper [11] consists of stainless-steel (SUS 316) tube of 10 mm in inner diameter (ID) and quartz reaction tube of 13 mm ID. The distances between V_1 and S (sample), and between V_1 and CM (capacitant manometer) are ca. 62 cm (32 cm SUS tube and 30 cm quartz tube) and 55 cm, respectively. Thus, the conductance from the sample and that from CM sensor are approximately the same and is as small as ca. 2.3×10^{-4} m^3/s. Because of the small conductance, the gas pressure measured by CM is about two orders of magnitude higher than that measured at the ion gauge located just onside of the turbo-molecular pump (see Fig. 2 of Ref. [11]). On the other hand, the gas pressures at the sample and CM sensor during vacuum pumping (dynamic vacuum) are approximately the same provided that the evolution of gases from the sample is as small as that from the CM wall. It is noted that the samples denoted as dynamic vacuum (listed in Table 1) were treated under such vacuum pumping conditions. Different from the sample treated under dynamic vacuum, the samples denoted as 1 Pa O_2 were treated under a

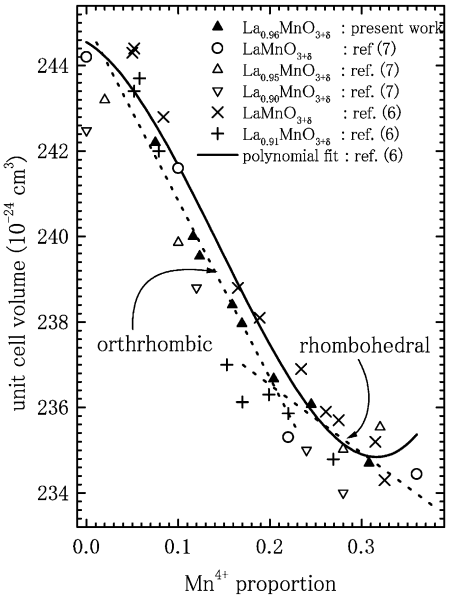

Fig. 1. Unit-cell volumes for $La_{1-\Delta}MnO_{3+\delta}$ are plotted as a function of Mn^{4+} proportion. The thick line is drawn by the third-order polynomial fit given in Ref. [6]. Note that the dotted lines in the orthorhombic and rhombohedral regions have different slope.

constant oxygen partial pressure controlled by the variable leak valve V3, and consequently the samples should have been equilibrated under an accurately defined partial pressure. The samples denoted as 135 and 1170 Pa were equilibrated under the closed system (enclosed by V_1 and V_2 in Fig. 2 of Ref. [11]) as shown by the desorption curves in Fig. 4 of Ref. [11].

The Mn^{4+} proportions of the samples were investigated by a combination of volumetric method combined with the unit cell volume as described in detail in the previous paper [11]. In this research we have also obtained similar $Mn^{4+}(\delta)$ vs. unit cell volume plots (Fig. 8 of Ref. [11]) for $La_{0.96}MnO_{3+\delta}$ samples, which are given in Fig. 1. Literature data [6,7] for unit-cell volume of $La_{1-\Delta}MnO_{3+\delta}$ are also plotted in the same figure. An examination of these data shows that the unit-cell volumes for orthorhombic and rhombohedral

regions have different δ dependency and can be approximated by two linear lines with different slope. The estimated Mn^{4+} concentrations listed in Table 1 were obtained from the two linear relations (dotted lines in Fig. 1). Magnetization measurements were made with a Quantum Design MPMS system, in a field of 500 Oe for temperature dependence, and at 10 K for field dependence.

3. Results

Figs. 2 and 3 show the temperature dependence of the magnetization and inverse magnetic susceptibility for the oxygen-annealed (in 10^5 Pa O_2) and oxygen-reduced (in 1 Pa O_2) $La_{0.7}Ca_{0.3}MnO_{3+\delta}$ and $La_{0.7}Sr_{0.3}MnO_{3+\delta}$ polycrystalline samples. Insets to the figures show the field dependence of the magnetization for the same samples. These magnetization data demonstrate that the oxygen-reduction treatment at 1273 K in 1 Pa O_2 affects a little on the magnetization properties. These observations are also consistent with the established experimental facts that in $La_{0.7}Sr_{0.3}MnO_{3+\delta}$, Mn^{4+}

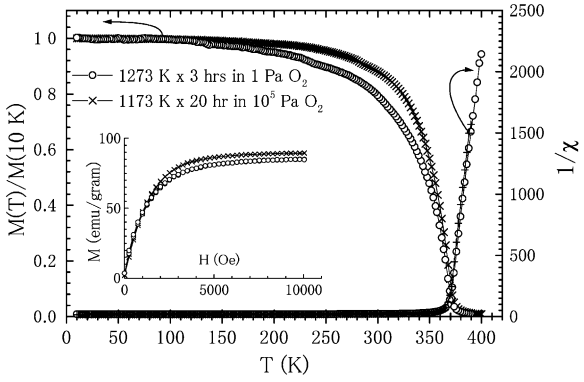

Fig. 2. Temperature dependence of magnetization (500 Oe) for $La_{0.7}Sr_{0.3}MnO_{3+\delta}$ annealed in different oxygen partial pressures (10^5 and 1 Pa).

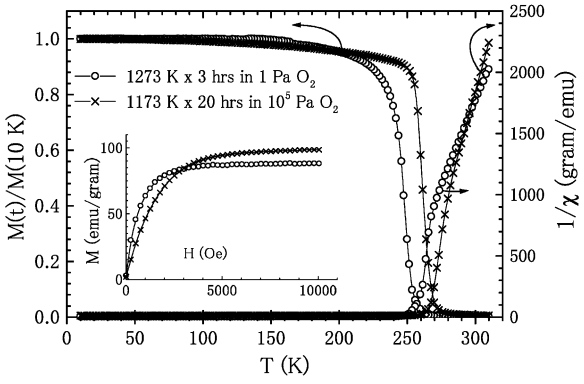

Fig. 3. Temperature dependence of magnetization (500 Oe) for $La_{0.7}Ca_{0.3}MnO_{3+\delta}$ annealed in different oxygen partial pressures (10^5 and 1 Pa).

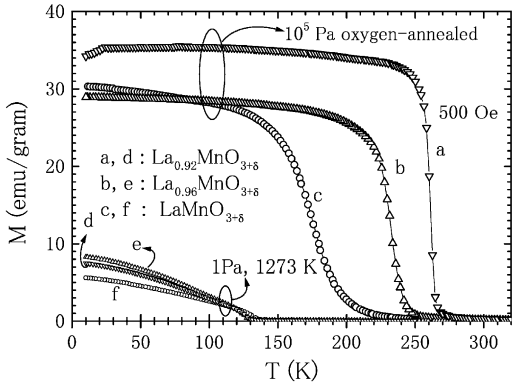

Fig. 4. Temperature dependence of magnetization (500 Oe) for $La_{1-\Delta}MnO_{3+\delta}$ ($1-\Delta = 1.0$, 0.96 and 0.92) annealed in different oxygen partial pressures (10^5 Pa: (a–c) and 1 Pa: (d–f)).

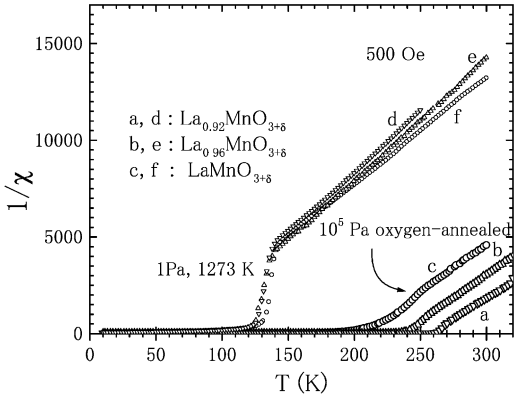

Fig. 5. Temperature dependence of inverse susceptibility (500 Oe) for $La_{1-\Delta}MnO_{3+\delta}$ ($1-\Delta = 1.0$, 0.96 and 0.92) annealed in different oxygen partial pressures (10^5 Pa: (a–c) and 1 Pa: (d, e)).

concentration is almost independent of oxygen partial pressure and kind of atmosphere during annealing [1,2,5] and oxygen stoichiometry around 3.0 is stable over a wide range of oxygen partial pressure.

Figs. 4–6 show the temperature and field dependence of the magnetization and inverse susceptibility for the oxygen-annealed (10^5 Pa O_2) and oxygen-reduced (1 Pa O_2) $La_{1-\Delta}MnO_{3+\delta}$ samples with $1-\Delta = 1.0$, 0.96 and 0.92. Comparisons of Figs. 2 and 3 with Figs. 4–6 show that the change in the magnetic properties is quite different between the Sr-, Ca-doped and La-deficient (vacancy doped according to the conventional terminology) compounds. In the La-deficient samples, the oxygen-reduced samples show almost the same magnetic properties independent of the La deficient (doping) level. From the field dependence of the magnetization curves in Fig. 6 (10 K), the magnetization at 10 kOe magnetic field for the as-prepared samples show almost the same values, 85–95 emu/g (19 600–21 500 emu/mol), i.e., 3.4–3.6 μ_B, which are close the expected value for full alignment of the spins (3.7 μ_B). This behavior could be expected from the fact

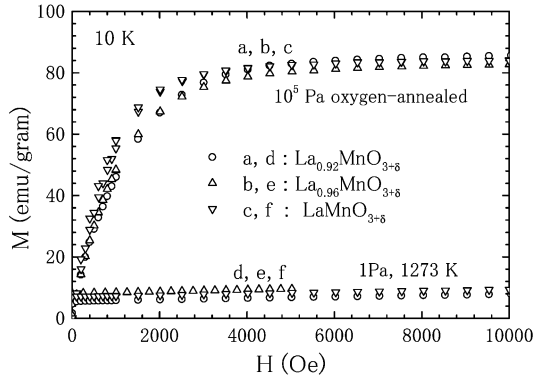

Fig. 6. Field dependence of magnetization at 10 K for $La_{1-\Delta}MnO_{3+\delta}$ ($1-\Delta=1$, 0.96 and 0.92) annealed in different oxygen partial pressures (10^5 Pa: (a–c) and 1 Pa: (d, e)).

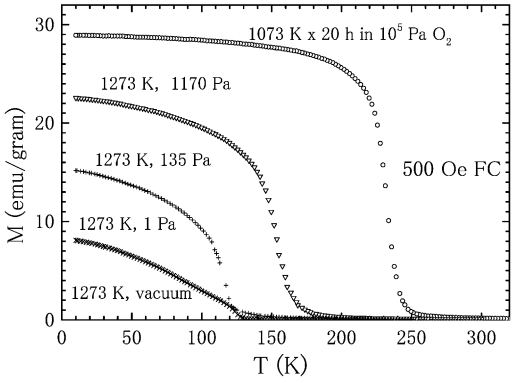

Fig. 7. Temperature dependence of magnetization for $La_{0.96}MnO_{3+\delta}$ annealed in different oxygen partial pressures and temperatures (10^5, 1170, 135, 1 Pa and dynamic vacuum).

that the maximum Mn^{4+} proportion for the samples is almost independent of the La-deficient level [3,7,8]. The contrasting decrease in the magnetization at 10 kOe and Curie temperature of the oxygen-reduced $La_{1-\Delta}MnO_{3+\delta}$ samples suggest that the Mn^{4+} vs. P_{O_2} relation must be essentially different from that of the Sr- and Ca-doped manganites.

Fig. 7 shows the temperature dependence of the magnetization for the $La_{0.96}MnO_{3+\delta}$ sample which underwent oxygen-reduction treatments in different oxygen partial pressures of 1170, 35 and 1 Pa and in a dynamic vacuum at 1273 K for 0.5–3 h. The figure shows a continuous decrease in the magnetization with decreasing oxygen partial pressure during the reduction treatments. The continuous change observed in the present samples is consistent with that for the $LaMnO_{3+\delta}$ and $LaMn_{0.97}O_{3+\delta}$ samples in which lattice parameters (unit-cell volume) and estimated Mn^{4+} proportion also change with changing desorption and absorption equilibrium pressures [11].

Table 1 summarizes details of the oxygen-reduction treatments, lattice parameters, unit-cell volume and estimated Mn^{4+} proportion for the La-deficient samples shown in Figs. 4–7. The magnetization and XRD data given in Figs. 4–7 and Table 1 strongly demonstrate that the Mn^{4+} concentration vs. oxygen equilibrium pressure relation, i.e., pressure, P, oxygen non-stoichiometry, δ and temperature, T (P–δ isotherms), must be different from those of Sr- and Ca-doped manganites. Taking into account the experimental facts that the enthalpy of oxygenation (vacancy formation $\Delta H_v/R$) for $La_{1-x}Sr_xMnO_{3+\delta}$ varies a little with changing Sr doping level x [3,5,10], it is hard to imagine that the change in the Mn^{4+} concentration for the La-deficient samples is due to the drastic change in the entropy and enthalpy of vacancy formation. In the next section, we will examine in detail about this problem.

4. Discussion

4.1. Solubility limit of La-deficient $La_{1-\Delta}MnO_{3+\delta}$

Before discussing various defect models for the La-deficient manganites, we must take care of the thermodynamic aspect that in $La_{1-\Delta}MnO_{3+\delta}$ with $1-\Delta$ greater than the non-stoichiometry limit of La to Mn ratio, $1-\Delta_L$, excess Mn, in principle, is segregated into Mn_3O_4 (or Mn_2O_3) according to

$$La_{1-\Delta}MnO_{3+\delta} = \frac{1-\Delta}{1-\Delta_L}La_{1-\Delta_L}MnO_{3+\delta} + \frac{\Delta-\Delta_L}{1-\Delta_L}\left(\frac{1}{3}Mn_3O_4 \text{ or } \frac{1}{2}Mn_2O_3\right), \quad (1)$$

where $\Delta_L \simeq 0.1$ according to the experimental data [6,7,13]. In the actual case, however, the equilibrium state described by the above equation is not always attained due to the small driving force necessary to attain equilibrium [14]. In the following, however, we assume that the equilibrium state described by Eq. (1) is always attained and Δ in $La_{1-\Delta}MnO_{3+\delta}$ must be smaller than Δ_L.

4.2. Defect models considering La site doping

As described above, the change in the Mn^{4+} concentration (excess oxygen δ) with increasing oxygen reduction is quite different between the La-deficient (vacancy doped) and Ca- and Sr-doped lanthanum manganites. If vacancies are doped in the La sites of the La-deficient manganite as expressed by the formula composition $La_{1-\Delta}V_\Delta MnO_{3+\delta}$, δ vs. equilibrium oxygen partial pressure relation is expected to behave similarly in the La-deficient and Ca- and Sr-doped manganites because thermodynamic parameters such as enthalpy of defect formation vary a little with changing doping level x [3,5,10]. To examine this problem in detail, let us

extend the defect model for $LaMnO_{3+\delta}$ [11] to the case where divalent cations and vacancies are doped in the La site. Here we assume that in $La_{1-x}M_xMnO_{3+\delta}$, excess oxygen generates vacancies both in the La and Mn sites with equal amounts according to

$$La_{1-x}M_xMnO_3+\frac{\delta}{2}O_2=\frac{3+\delta}{3}\left\{(La_{1-x}M_x)^{3+}_{\frac{3}{3+\delta}}V_{\frac{\delta}{3+\delta}}\right\}\times\left\{Mn^{3+}_{\frac{3(1-2\delta-x)}{3+\delta}}Mn^{4+}_{\frac{3(2\delta+x)}{3+\delta}}V_{\frac{\delta}{3+\delta}}\right\}O_3 \quad (2)$$

and, similarly for $La_{1-\Delta}V_\Delta MnO_{3+\delta}$

$$La_{1-\Delta}V_\Delta MnO_3+\frac{\delta}{2}O_2=\frac{3+\delta}{3}\left\{La^{3+}_{\frac{3-3\Delta}{3+\delta}}V_{\frac{\delta+3\Delta}{3+\delta}}\right\}\times\left\{Mn^{3+}_{\frac{3(1-2\delta-3\Delta)}{3+\delta}}Mn^{4+}_{\frac{3(2\delta+3\Delta)}{3+\delta}}V_{\frac{\delta}{3+\delta}}\right\}O_3. \quad (3)$$

Upon dissolution of 3/2 oxygen molecules, therefore, six Mn^{4+} ions and two vacancies, i.e., one each at La (V_{La}) and Mn (V_{Mn}) sites are formed according to

$$6Mn^{3+}+\frac{3}{2}O_2=6Mn^{4+}+3O^{2+}+V_{La}+V_{Mn} \quad (4)$$

and the chemical potential of three oxygen ions for $La_{1-x}M_xMnO_{3+\delta}$, which is in equilibrium with $(3/2)O_2$ molecules in the gas phase can be expressed as

$$3\mu_O=3\mu_O^0(T)+RT\ln\left\{\frac{\eta\delta/(3+\delta)}{1-\eta\delta/(3+\delta)}\right\}^2+RT\ln\left(\frac{2\delta+x}{1-2\delta-x}\right)^6=3\mu_O^0(T)+RT\ln f(\delta) \quad (5)$$

and the corresponding equation for $La_{1-\Delta}V_\Delta MnO_{3+\delta}$ is given by

$$3\mu_O=3\mu_O^0(T)+RT\ln\left[\left\{\frac{\eta(\delta+3\Delta)/(3+\delta)}{1-\eta(\delta+3\Delta)/(3+\delta)}\right\}_{La}\times\left\{\frac{\eta\delta/(3+\delta)}{1-\eta\delta/(3+\delta)}\right\}_{Mn}\right]+RT\ln\left(\frac{2\delta+3\Delta}{1-2\delta-3\Delta}\right)^6=3\mu_O^0(T)+RT\ln f(\delta), \quad (6)$$

where $\Delta=\Delta_L$ for $\Delta\geqslant\Delta_L$. The first term in the middle expression of Eqs. (5) and (6), $3\mu_O^0(T)$ is the standard potential at temperature T. The second term of Eqs. (5) and (6) arises from the entropy of mixing of La and Mn site vacancies. Here we assume that excess oxygen δ generates equal amounts of vacancies both in the La and Mn sites, and the total vacancy proportions in the La and Mn sites are equal in Eqs. (2) and (5) but different in Eqs. (3) and (6). This is because in Eqs. (3) and (6), vacancies caused by the La deficiency $3\Delta/(3+\delta)$ are added in addition to the vacancies generated by the excess oxygen, $\delta/(3+\delta)$. In Eq. (6) subscripts La and Mn mean that the entropies of mixing of vacancies for La and Mn sites are different. The third term in Eqs. (5) and (6) comes from the entropy of mixing of Mn^{4+} ions, in which Mn^{4+} proportions increase from 2δ to $2\delta+x$ and 2δ to $\delta+3\Delta$ for $La_{1-x}M_xMnO_{3+\delta}$ and $La_{1-\Delta}V_\Delta MnO_{3+\delta}$, respectively. The parameter η is adjustable; it can be determined experimentally from the maximum excess oxygen value δ_{max} [11]. The parameter $\eta=(3+\delta_{max})/\delta_{max}$ in Eq. (5) depends on x as well as on Δ in Eq. (6). The δ_{max} value is known to decreases with increasing x [3,10]. At the equilibrium, we have

$$\frac{3}{2}\mu_{O_2}=\frac{3}{2}\mu_{O_2}^0(T)+RT\ln P_{O_2}^{3/2}=3\mu_O, \quad (7)$$

where μ_{O_2} and $\mu_{O_2}^0(T)$ are the oxygen molecule chemical potential in the gas phase at temperature T and its standard potential, respectively. From Eqs. (5)–(7), the equilibrium constant K becomes

$$K=\exp\left\{\frac{(3/2)\mu_{O_2}^0(T)-3\mu_O^0(T)}{RT}\right\}=f(\delta)P_{O_2}^{-3/2}. \quad (8)$$

In Fig. 8, equilibrium pressures at 1073–1273 K calculated using Eqs. (5) and (8) are drawn against δ ($\delta>0$ region) for $La_{1-x}Sr_xMnO_{3+\delta}$ with $x=0$ and 0.3, respectively. In the same figure, experimental data obtained from thermo-gravimetric [2,15] and volumetric [11] methods are also plotted. In this calculation, equilibrium constant K and parameter η for $x=0$ were taken from those for the calculated desorption isotherms given in the previous paper [11], i.e., $\ln K=45\,700/T-40.0$ and $\eta=17.67$, respectively. As for $La_{1-x}Sr_xMnO_{3+\delta}$, the maximum excess oxygen values, δ_{max}, have been shown to decrease with increasing Sr

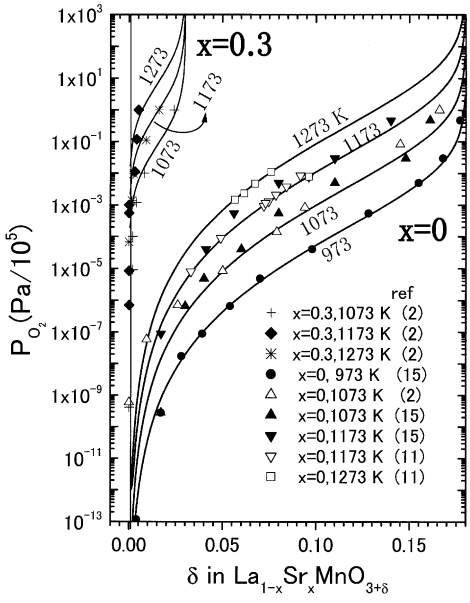

Fig. 8. Calculated (thick lines) and observed P–δ isotherms (973–1273 K) for $LaMnO_{3+\delta}$ ($x=0$) and $La_{0.7}Sr_{0.3}MnO_{3+\delta}$ ($x=0.3$).

doping level [1,3,10], i.e., δ_{max} value decreases from 0.18–0.17 for $x=0$ to 0.05–0.015 for $x=0.3$. In the above calculation we tentatively assumed a simple relation that $\delta_{max}=0.18-x/2$. This simple relation gives $\delta_{max}=0.03$ for $x=0.3$, i.e., $\eta=(3+\delta_{max})/\delta_{max}=101$. The agreements between the experimental and calculated values given in Fig. 8 are satisfactory in both $x=0$ and 0.3 cases. The most significant feature of the observed and calculated P–δ relation is nearly a vertical decrease in the equilibrium pressure around $\delta=0$. From the second term in the middle of Eq. (5), the sharp, vertical decrease in the isotherm curves can be interpreted in terms of the contribution of entropy of mixing of vacancies in the La and Mn sites, which approaches $RT\ln(\eta\delta/3)^2\rightarrow RT\ln(0)^2$ with δ approaching zero.

Fig. 9 shows the contribution of partial configurational entropy terms, $-\exp(\bar{S}_c/R)$ for $La_{1-x}Sr_xMnO_{3+\delta}$ and $La_{1-\Delta}V_\Delta MnO_{3+\delta}$ calculated from Eqs. (5) and (6) using the relation

$$-\frac{\bar{S}_c}{R}=\frac{3\mu_O-3\mu_O^0(T)}{RT}=\ln f(\delta). \tag{9}$$

In the present case, we used $\eta=101$ for $x=0.3$, $\eta=29.6$ for $x=0.15$ according to the simple relation cited above. As for the La-deficient manganites we also assume $\delta_{max}=0.18-3\Delta/2$ and $(\eta=(3+\delta_{max})/(\delta_{max}+3\Delta)$. These relations give $\eta=9.18$, 12.7 and 17.67 for $\Delta=0.1$, 0.05 and 0.0, respectively. Similar $\bar{S}_c$ vs. δ relations in the Sr-doped and La-deficient manganites shown in the figure suggest that Mn^{4+} proportion in the La-deficient case should converge to the different

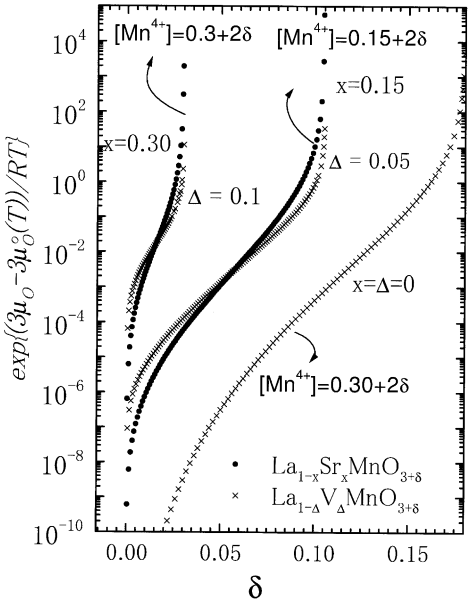

Fig. 9. Calculated partial configurational entropy terms, $f(\delta)=\exp(-\bar{S}_c/R)=\exp\{(3\mu_O-3\mu_O^0(T))/RT\}$ for $La_{1-\Delta}V_\Delta MnO_{3+\delta}$ ($\Delta=0.0$, 0.05 and 0.1). For comparison, corresponding curves for $La_{1-x}Sr_xMnO_{3+\delta}$ ($x=0.15$ and 0.3) are plotted in the same figure.

values characteristics of La-deficient (vacancy doped) level, i.e., 0.3 for $\Delta=0.1$, 0.15 for $\Delta=0.05$ and 0 for $\Delta=0$. These estimated values are different from the observed magnetization and lattice constant data (see Figs. 4–7 and Table 1) that the Mn^{4+} proportion for the oxygen-reduced samples converges to the same value $\simeq$0.02–0.04, independent of the initial La-deficient (vacancy doping) level. Thus, the assumption that vacancies locate in the La sites fails to explain the contrasting behavior against the reduction of oxygen. Thus we need to examine another defect model compatible with the observed contrasting behavior cited above.

4.3. Defect models considering Mn_3O_4 segregation and Mn enters into La site in the $\delta<0$ region

In discussing defect models, we are not concerned with the oxygen site vacancy formation which is known to occur at extremely lower oxygen partial pressures as 10^{-10}–10^{-5} Pa which is at least 10^5 orders of magnitude lower than the pressure range (10^5–1 Pa) treated in the present case. In this section, we shall examine models 1 and 2 of the following three models.

Model 1: In the $\delta<0$ region Mn_3O_4 (Mn_2O_3) must be segregated to compensate the decrease in the La site vacancy concentration.

Model 2: In the $\delta<0$ region, Mn ions enter into the La sites to compensate the decrease in the La site vacancy concentration.

Model 3: In the $\delta>0$ region, as well as in the $\delta<0$ region, Mn ions enter into the La sites to create Mn site vacancies and the amount of Mn ions in the La sites keeps constant value with the variation of δ for the entire δ region. This model will be discussed in the next section.

First of all we assume that in the $\delta>0$ region, excess oxygen generates equal amounts of vacancies both in the La and Mn sites. Thus, for the $\delta>0$ region, models 1 and 2 assume the same equations with those for the La site vacancy model described above (Eqs. (3) and (6)). As for the $\delta<0$ region, Eq. (3) shows that vacancy proportion in the Mn site, $\delta/(3+\delta)$, becomes zero and consequently model 2 needs segregation of Mn_3O_4 to compensate the decrease in the La site vacancies according to

$$La_{1-\Delta}V_\Delta MnO_3-\frac{5}{6}\Delta O_2 = (1-\Delta)LaMnO_3+\frac{\Delta}{3}Mn_3O_4 \quad (\delta<0). \tag{10}$$

The decomposition reaction expressed by Eq. (10) proceeds, however, under a constant decomposition pressure, P_d, until the initial compound $La_{1-\Delta}V_\Delta MnO_3$ completely decomposes into the resultant products, $(1-\Delta)LaMnO_3+(\Delta/3)Mn_3O_4$. This implies that

during the decomposition reaction, only two lanthanum manganite species with compositions, $La_{1-\Delta}V_{\Delta}MnO_3$ and $LaMnO_3$ are found from $\delta \simeq 0$ to $\delta = -3\Delta/2$ region. This model, however, cannot reasonably explain the experimental facts that in $La_{1-\Delta}MnO_3$, various Mn^{4+} proportion between $\simeq 0$ to $\simeq 0.33$ and a continuous lattice parameter change from rhombohedral to orthorhombic structure have been observed [6–8]. It should be also noted that three phase coexisting state corresponding to a mixture of $La_{1-\Delta}MnO_3$, $LaMnO_{3+\delta}$ and $Mn_3O_4(Mn_2O_3)$ phases has never been reported up to the present for the samples which underwent various oxygen-reduction treatments. Thus, this model should be completely ruled out.

Now let us examine model 2. According to this model Mn ions enter into the La sites in the $\delta<0$ region according to

$$La_{1-\Delta}V_{\Delta}MnO_3 + \frac{\delta}{2}O_2 = \frac{3+\delta}{3}\left\{La_{\frac{3(1-\Delta)}{3+\delta}}Mn_{\frac{-\delta}{3+\delta}}V_{\frac{3\Delta+2\delta}{3+\delta}}\right\}MnO_3 \quad (\delta<0) \tag{11}$$

and in terms of species participating in the reaction

$$6Mn^{4+} + 2Mn^{3+}(\text{Mn site}) + 2V_{La} - \frac{3}{2}O_2 = 6Mn^{3+} + 2Mn^{3+}(\text{La site}) - 3O^{2-} \quad (\delta<0). \tag{12}$$

Since $\delta<0$ in Eq. (11), $+(\delta/2)O_2$ in the equation means loss of oxygen from $La_{1-\Delta}V_{\Delta}MnO_3$. Thus, instead of decreasing the La site vacancy proportion, $(3\Delta+2\delta)/(3+\delta)$, (since $\delta<0$, $3\Delta+2\delta<3\Delta$ in the $\delta<0$ region) La site Mn ion proportion, $-\delta/(3+\delta)$ increases with increasing $|\delta|$ ($\delta<0$). This situation is similar to that found in the oxygen site vacancies introduced in the $\delta<0$ region for $LaMnO_{3+\delta}$ and Sr- and Ca-doped $La_{1-x}M_xMnO_{3+\delta}$ [3,10,16], where vacancy proportion in the oxygen site increases with increasing $|\delta|$ ($\delta<0$). For the above model the partial molar configurational entropy arising from vacancies and Mn ions in the La sites is expressed as

$$-\frac{\bar{S}_c}{R} = \ln\left\{\frac{\eta(3\Delta+2\delta)/(3+\delta)}{1-\eta(3\Delta+2\delta)/(3+\delta)}\right\}^2 + \ln\left\{\frac{(1+\delta)/(3+\delta)}{-\delta/(3+\delta)}\right\}^2 = \ln f(\delta) \quad (\delta<0). \tag{13}$$

The second term of the middle of the above equation is the configurational entropy arising from Mn ions in the La sites. Fig. 10 shows plots of $-\bar{S}_c/R$ against δ in the $\delta<0$ region. This figure shows two step nearly vertical decrease at $\delta = 0$ and $-2\Delta/3$, respectively (two plateaus when δ plotted against P_{O_2}). This behavior, however, is not consistent with the present observation that there is no vertical decrease in P_{O_2} around the $\delta = 0$ region.

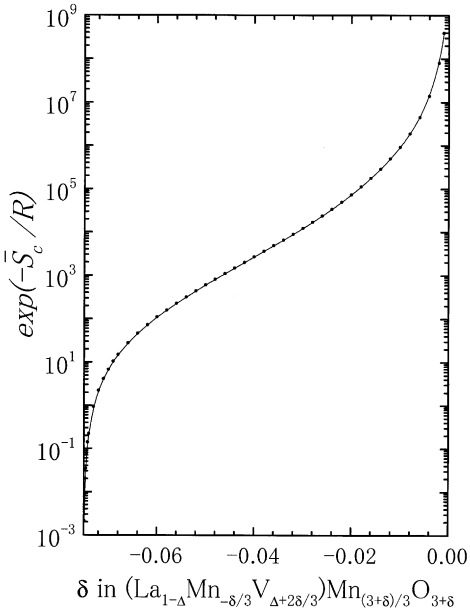

Fig. 10. Plots of $f(\delta) = \exp(-\bar{S}_c/R)$ as a function of δ for model 2 ($-\delta/3$ Mn ions enter into the La sites in compensation for the disappearance of $-\delta/3$ vacancies in the La sites for $\delta<0$ region).

4.4. La and Mn site vacancy model

As described above models 1 and 2 have failed to explain the continuous change in the Mn^{4+} proportion across the $\delta = 0$ region. The reduction in the Mn^{4+} proportion which is independent of La-deficient level strongly suggests that vacancies caused by the La deficiency should exist not only in the La sites but also in the Mn sites. In other words, residual vacancies exist in the Mn sites even at $\delta<0$ region. Thus in model 3, it is assumed that in $La_{1-\Delta}MnO_{3+\delta}(\Delta \leqslant \Delta_{max} \simeq 0.1)$, Δ_2 Mn atoms ($\Delta_2<\Delta$) enter into the La sites to create Δ_2 and $\Delta_1 = \Delta - \Delta_2$ vacancies in the Mn and La sites, respectively, according to:

$$La_{1-\Delta}MnO_3 \rightarrow \{La_{1-\Delta}Mn_{\Delta_2}V_{\Delta_1}\}\{Mn_{1-\Delta_2}V_{\Delta_2}\}O_3. \tag{14}$$

In this case, vacancies from the excess oxygen δ and those from the La deficiency, Δ_1 and Δ_2, are distributed in the La and Mn sites according to

$$\{La_{1-\Delta}Mn_{\Delta_2}V_{\Delta_1}\}\{Mn_{1-\Delta_2}V_{\Delta_2}\}O_3 + \frac{\delta}{2}O_2 = \frac{3+\delta}{3}\left\{La_{\frac{3(1-\Delta)}{3+\delta}}Mn_{\frac{3\Delta_2}{3+\delta}}V_{\frac{3\Delta_1+\delta}{3+\delta}}\right\} \times \left\{Mn^{3+}_{\frac{3(1-3\Delta-\Delta_2-2\delta)}{3+\delta}}Mn^{4+}_{\frac{3(3\Delta+2\delta)}{3+\delta}}V_{\frac{3\Delta_2+\delta}{3+\delta}}\right\}O_3, \tag{15}$$

where $3\Delta_1+\delta \geqslant 0$ (or $3\Delta_2+\delta \geqslant 0$) in the above equation. The reacting species participating in the above reaction are the same as those given in Eq. (4), and the

partial molar entropy of mixing of vacancies, $\bar{S}_c^V$ is given by

$$\bar{S}_c^V = -R\ln\left\{\frac{\eta(3\Delta_1+\delta)/(3+\delta)}{1-\eta(3\Delta_1+\delta)/(3+\delta)}\right\}_{\mathrm{La}} - R\ln\left\{\frac{\eta(3\Delta_2+\delta)/(3+\delta)}{1-\eta(3\Delta_2+\delta)/(3+\delta)}\right\}_{\mathrm{Mn}} \quad (16)$$

and the partial molar entropy of mixing of Mn^{4+}, $\bar{S}_c^{\mathrm{Mn}}$, is given by

$$\bar{S}_c^{\mathrm{Mn}} = -R\ln\left\{\frac{3\Delta+2\delta}{1-3\Delta-\Delta_2-2\delta}\right\}^6. \quad (17)$$

In the above equation we use an approximation that only Δ_2 Mn^{3+} ions enter into the La sites. This approximation could be justified by considering the difference in the ionic radius of Mn^{3+} with that of Mn^{4+}. The larger ionic radius and 3+ valence might be the possible cause of Mn^{3+} ions in the La sites. Then the chemical potential $3\mu_{\mathrm{O}}$ is given by

$$3\mu_{\mathrm{O}} = 3\mu_{\mathrm{O}}^0(T) - T(\bar{S}_c^V + \bar{S}_c^{\mathrm{Mn}}) = 3\mu_{\mathrm{O}}^0(T) + RT\ln f(\delta). \quad (18)$$

The partial entropy term, $\ln f(\delta) = -(\bar{S}_c^V + \bar{S}_c^{\mathrm{Mn}})/R$, in the middle of the above equation behave differently when $\ln f(\delta)$ is plotted against δ, especially in the vicinity of $\delta \simeq 0$ region. The vacancy concentrations, $(3\Delta_1+\delta)/(3+\delta)$ and $(3\Delta_2+\delta)/(3+\delta)$ given in Eq. (16) and the Mn^{4+} concentration, $3\Delta+2\delta$, given in Eq. (17), do not approach zero with δ approaching zero because of the contribution from both the La and Mn site residual vacancies, Δ_1 and Δ_2, and the residual Mn^{4+} concentration, 3Δ. In this case, the vacancy concentrations in the La and Mn sites become zero when $\delta+3\Delta_1=0$ or $\delta+3\Delta_2=0$, i.e., $\delta=-3\Delta_1$ or $\delta=-3\Delta_2$. Thus the P–δ isotherm has a sharp decrease with δ approaching $-3\Delta_1$ or $-3\Delta_2$ depending on the relative magnitude of Δ_1 and $\Delta-\Delta_1=\Delta_2$. If $\Delta_1=\Delta_2$, calculated P–δ relation has a sharp decrease at $\delta=1.5\Delta$.

Figs. 11 and 12 show how the Mn ion proportion entering into the La site, Δ_2 affect the P_{O_2} vs. δ (or $[Mn^{4+}]$) relation at 1273 K for $La_{0.96}MnO_{3+\delta}$ and $La_{0.92}MnO_{3+\delta}$, respectively. In this calculation using Eqs. (16)–(18), we assumed $\delta_{\max}=0.18-(3/2)\Delta$, $3\Delta_2+\delta_{\min}=0$, $\eta=(3+\delta_{\max})/(3\Delta_1+\delta_{\max})$ and $\ln K=-4.2$ at 1273 K ($\ln K = 45\,800/T-40.0$). Table 2 shows combinations of these parameters used in the calculation of P–δ–T relation shown in Figs. 11 and 12. From the figure one can see that the calculated isotherms show a sharp, nearly vertical decrease in P_{O_2} at $\delta_{\min}=-3\Delta_2$ ($\Delta_2<\Delta_1$), and the onset pressure of this vertical decrease increases with decreasing La site Mn substitution Δ_2. Another remark obtained from the figure is that the difference between $\delta_{\max}$ and $\delta_{\min}$ seems to be a good indication to determine Δ_2. From Figs. 4–7 and Table 1, one can roughly estimate Δ_2 value. For example, the

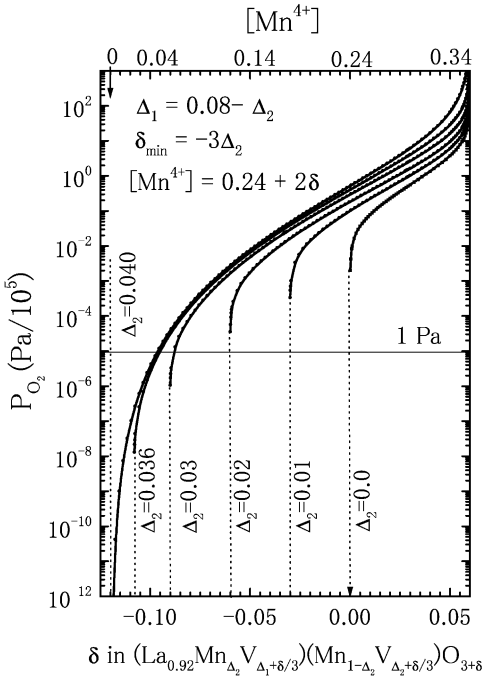

Fig. 11. Calculated Δ_2 dependence of P–δ isotherms for $La_{0.92}MnO_{3+\delta}$ assuming Δ_2 $(=0.08-\Delta_1)$ Mn ions enter into the La sites to create $\{La_{0.92}Mn_{\Delta_2}V_{\Delta_1+\delta/3}\}\{Mn_{1-\Delta_2}V_{\Delta_2+\delta/3}\}O_{3+\delta}$ formula composition.

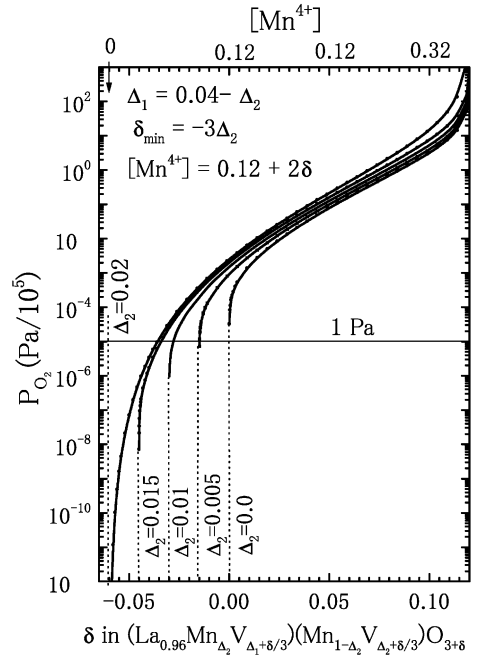

Fig. 12. Calculated Δ_2 dependence of P–δ isotherms for $La_{0.96}MnO_{3+\delta}$ assuming Δ_2 $(=0.04-\Delta_1)$ Mn ions enter into the La sites to create $\{La_{0.96}Mn_{\Delta_2}V_{\Delta_1+\delta/3}\}\{Mn_{1-\Delta_2}V_{\Delta_2+\delta/3}\}O_{3+\delta}$ formula composition.

magnetization vs. temperature curves in Fig. 7 and the estimated Mn^{4+} proportions (from the unit-cell volume) in Table 1, show that the Mn^{4+} proportion is almost the same for the $La_{0.92}MnO_{3+\delta}$ and $La_{0.96}MnO_{3+\delta}$ samples oxygen-reduced in 1 Pa O_2 and in dynamic vacuum.

Table 2
Combinations of Δ_1, $\Delta_2 = \Delta - \Delta_1$, η and δ_{min} used for the P–δ isotherms in Figs. 11 ($\Delta = 0.08$) and 12 ($\Delta = 0.04$)

$\Delta = 0.08$, $\delta_{max} = 0.06$				$\Delta = 0.04$, $\delta_{max} = 0.12$			
Δ_1	Δ_2	η	δ_{min}	Δ_1	Δ_2	η	δ_{min}
0.08	0	10.2	0	0.04	0	13.0	0
0.07	0.01	11.33	−0.03	0.035	0.005	13.87	−0.015
0.06	0.02	12.75	−0.06	0.030	0.01	14.86	−0.03
0.05	0.03	14.57	−0.09	0.025	0.015	16.00	−0.045
0.044	0.036	15.97	−0.108	0.02	0.02	17.33	−0.06
0.04	0.04	17.0	−0.12				

This suggests that the onset pressure of the nearly vertical decrease should be located close to P_{O_2} of 1 Pa. At the same time, the estimated Mn^{4+} proportion equilibrated in 1 Pa and in dynamic vacuum is around 0.07, which corresponds to $\Delta_2 \simeq 0.03$ for the isotherm curves of $La_{0.92}MnO_{3+\delta}$ (Fig. 11) and to $\Delta_2 \simeq 0.01$ for that of $La_{0.96}MnO_{3+\delta}$ (Fig. 12), respectively.

From the estimated Δ_2 values cited above, one can evaluate net proportion of vacancies in the La sites, $\Delta_1 - \Delta_2 \simeq 0.02$ for both $La_{0.92}MnO_{3+\delta}$ and $La_{0.96}MnO_{3+\delta}$, respectively. If we take into account the net proportion of vacancies in the La sites, $La_{1-\Delta}MnO_{3+\delta}$ formula can be better expressed as

$$\begin{aligned} &La_{1-\Delta}MnO_{3+\delta} \\ &= \{La_{1-\Delta}Mn_{\Delta_2}V_{\Delta_1}\}\{Mn_{1-\Delta_2}V_{\Delta_2}\}O_{3+\delta} \\ &= (1-\Delta_2)\left\{La_{\frac{1-\Delta}{1-\Delta_2}}Mn_{\frac{\Delta_2}{1-\Delta_2}}V_{\frac{\Delta_1-\Delta_2}{1-\Delta_2}}\right\}MnO_{3+\frac{\delta+3\Delta_2}{1-\Delta_2}}. \end{aligned} \quad (19)$$

This equation means that the net excess oxygen in $La_{1-\Delta}MnO_{3+\delta}$ is not δ but $(\delta + 3\Delta_2)/(1-\Delta_2)$. This also means that the increase in the Mn^{4+} proportion due to the net vacancy doping, $3(\Delta_1 - \Delta_2)/(1-\Delta_2) \simeq 3(\Delta_1 - \Delta_2)$ (see Eq. (19)) lies around 0.06, which is smaller than the expected value $3\Delta = 0.24$ for $La_{0.92}MnO_{3+\delta}$ and 0.12 for $La_{0.96}MnO_{3+\delta}$ assuming full vacancy doping. Thus it seems to be reasonable to consider that the change in the magneto-transport properties caused by the increase in the La-deficient level is not due to the vacancy doping in the La site but due to the excess Mn atoms entering in the La sites, which play an important role to keep complete Mn–O–Mn plane. Thermodynamic treatments of this picture are now in progress.

So far it has been implicitly accepted that in the La-deficient manganites, vacancies are located in the La sites, and the above model that Mn^{3+} ions enter into the La sites to give both La and Mn site vacancies seems to be not common. A question arises that the ionic radius of Mn^{3+} ion is too small to fit the La site. It should be emphasized, however, that the maximum solid solubility of Mn^{3+} ion in the La site, 0.04, is still significantly smaller than that of vacancy in the La site, 0.0566. If one assume that, in the $\Delta = 0.08$ composition, 0.03 Mn^{3+} ions enter into the La sites, the vacancy proportion decreases from the unacceptable level 0.08 (>0.0566) to the acceptable level 0.05 (<0.0566). From the thermodynamic point of view, the amounts of substitution of the La site vacancies with Mn ions are evaluated by the energy balance between the vacancy formation and Mn substitution. Thus, the equilibrium Δ_1 and Δ_2 values are determined by the free energy minimum criterion in the $\Delta_2 = \Delta - \Delta_1$ vs. free energy curve. Fig. 13 shows a schematic diagram of the free energy for the vacancy doped and partially doped manganites vs. Mn/(La + Mn) ratio. At the Mn/(La + Mn) ratio of 0.5 ($\Delta = 0$), the free energy values for the two structures coincide, but with increasing Mn proportion, the free energy curves for the structure in which Mn ions enter into the La sites becomes stable than that for the vacancy fully doped structure $La_{1-\Delta}V_{\Delta}MnO_{3+\delta}$. The solubility limit of Mn ions in the La sites is determined from the co-tangent line connecting the two curves for $\{La_{1-\Delta}Mn_{\Delta_2}V_{\Delta_1+\delta/3}\}\{Mn_{1-\Delta_2}V_{\Delta_2+\delta/3}\}O_{3+\delta}$ and Mn_3O_4 (or Mn_2O_3) as schematically shown in the figure.

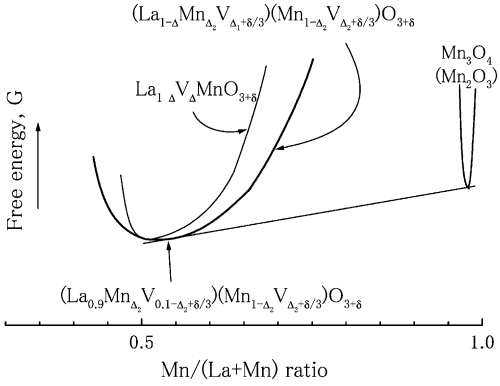

Fig. 13. A schematic diagram showing the change in free energy vs. Mn/(La + Mn) ratio in the $La_2O_3 - Mn_2O_3$ phase diagram. With Mn ions entering into the La sites, free energy at $\Delta \geqslant 0$ region becomes lower than the case without substitution as shown in the figure. The co-tangent line connecting the two curves shows minimum free energy line corresponding to the two phase coexisting region, i.e., $\frac{3}{3+\delta}\{La_{1-\Delta}Mn_{\Delta_2}V_{\Delta_1+\delta/3}\}\{Mn_{1-\Delta_2}V_{\Delta_2+\delta/3}\}O_{3+\delta} + Mn_3O_4$ (or Mn_2O_3).

5. Summary

The magnetic properties of the La-deficient manganites, $La_{1-\Delta}MnO_{3+\delta}$ depend strongly on the oxygen-reduction treatments. In agreement with the reported behavior of divalent cation doped manganites, $La_{1-x}M_xMnO_{3+\delta}$ (M: Sr, Ca) shows almost independent of the similar oxygen reduction treatments. In order to account for the observed contrasting oxygen-reduction effects, several models have been examined. It is concluded that in the $La_{1-\Delta}MnO_{3+\delta}$ formula composition, Δ_2 of Mn ions enter into the La sites to create both the La and Mn site vacancies, i.e., $\Delta_1 = \Delta - \Delta_2$ in the La and Δ_2 in the Mn sites. Thus the formula composition of the La-deficient manganites can be best expressed according to Eq. (15). This proposed model can explain the observed contrasting transport behavior with the reduction of oxygen and also the observed P–δ isotherms for $La_{1-\Delta}MnO_{3+\delta}$ with $\Delta =$ 0.05 and 0.1 (14).

Acknowledgment

The author wish to acknowledge Keiichi Ogawa, Rector of Yokohama City University, for his support for this research.

References

[1] I.G. Krogh Andersen, E. Krogh Andersen, P. Norby, E. Skou, J. Solid State Chem. 113 (1994) 320.
[2] J. Mizusaki, Y. Yonemura, H. Kamata, K. Ohyama, N. Mori, H. Takai, H. Tagawa, M. Dokiya, K. Naraya, T. Sasamoto, H. Inaba, T. Hashimoto, Solid State Ion. 132 (2000) 167.
[3] J.A.M. Roosmalen, E.H.P. Cordfunke, J. Solid State Chem. 110 (1994) 106, 109, 113.
[4] K. Nakamura, M. Xu, M. Klaeser, G. Linker, J. Solid State Chem. 156 (2001) 143.
[5] J.H. Kuo, H.U. Anderson, D.M. Sparlin, J. Solid State Chem. 83 (1989) 52.
[6] J.A.M. Roosmalen, D. van Vlaaderen, E.H.P. Cordfunke, W.L. Ljdo, D.J.W. Ijdo, J. Solid State Chem. 114 (1995) 516.
[7] J. Toepfer, J.B. Goodenough, Chem. Mater. 9 (1977) 1467.
[8] J. Toepfer, J.B. Goodenough, J. Solid State Chem. 130 (1997) 117.
[9] B.C. Tofield, W.R. Scott, J. Solid State Chem. 10 (1974) 183.
[10] J. Mizusaki, N. Mori, H. Takai, Y. Yonemura, H. Minamiue, H. Tagawa, M. Dokiya, H. Inaba, K. Naraya, T. Sasamoto, T. Hashimoto, Solid State Ion. 129 (2000) 163.
[11] K. Nakamura, K. Ogawa, J. Solid State Chem. 163 (2002) 65.
[12] K. Nakamura, K. Ogawa, J. Appl. Phys. 92 (2002) 6684.
[13] Y. Takeda, S. Nakai, T. Kojima, R. Kanno, N. Imanishi, G.Q. Shen, O. Yamamoto, M. Mori, C. Asakawa, T. Abe, Mater. Res. Bull. 26 (1991) 153.
[14] K. Nakamura, X. Liu, Z. Jiao, Trans. Russ. Acad. Sci. 65 (2001) 817.
[15] J. Mizusaki, H. Tagawa, Y. Yonemura, H. Minamiue, H. Nambu, Proceedings of the Second International Symposium on Ionic and Mixed Conducting Ceramics, Proceedings, Vol. 94-12, The Electrochemical Society, Inc., NJ, 1994, p. 402.
[16] J. Nowotny, M. Rekas, J. Am. Ceram. Soc. 81 (1998) 67.